PHYSICAL REVIEW C **82**, 014315 (2010)

Separable form of a low-momentum realistic NN interaction

P. Grygorov, E. N. E. van Dalen, and H. Müther
Institut für Theoretische Physik, Universität Tübingen, D-72076 Tübingen, Germany

J. Margueron
Institut de Physique Nucléaire, Université Paris-Sud, F-91406 Orsay CEDEX, France
(Received 22 March 2010; revised manuscript received 26 May 2010; published 26 July 2010)

The low-momentum interaction $V_{\text{low-}k}$ derived from realistic models of the nucleon-nucleon interaction is presented in a separable form. This separable force is supported by a contact interaction to achieve the saturation properties of symmetric nuclear matter. Bulk properties of nuclear matter and finite nuclei are investigated for the separable form of $V_{\text{low-}k}$ and two different parametrizations of the contact term. The accuracy of the separable force in Hartree-Fock calculations with respect to the original interaction $V_{\text{low-}k}$ is discussed. For a cutoff parameter Λ of 2 fm^{-1}, a representation by a rank-2 separable force yields sufficient accuracy, while higher ranks are required for larger cutoff parameters. The resulting separable force is parametrized in a simple way to allow for an easy application in other nuclear structure calculations.

DOI: 10.1103/PhysRevC.82.014315 PACS number(s): 21.60.Jz, 21.30.Fe, 21.65.−f, 26.60.−c

I. INTRODUCTION

The evaluation of bulk properties of finite nuclei and nuclear matter that starts from realistic models of the nucleon-nucleon (NN) interaction is a major challenge in modern nuclear physics. Since the exact form of the interaction resulted from the underlying theory of the strong interaction remains unknown, one usually has to deal with realistic models developed so as to fit experimental data for free NN scattering up to the threshold for pion production and properties of the deuteron [1–4]. It was performed by obtaining a best fit for a large number of adjustable parameters by using several thousands of experimental points so that there existed several quite different potential models, which were commonly used. A general feature of such realistic interactions is strong short-range and tensor components, which cannot be handled within the standard perturbation theory. Different approaches have been suggested to overcome this problem: the Bethe-Brueckner-Goldstone expansion [5], the correlated basis functions [6], the quantum Monte Carlo [7], and the self-consistent Green's function theory (see, e.g., Ref. [8]). These methods were successfully applied to describe bulk properties of nuclear matter [9], pairing gaps of nucleons [10], weak response [11], and shear viscosity of nuclear matter [12]. However, these approaches remain very complex to be applied directly to a description of finite nuclei, as well as inhomogeneous nuclear matter, also known as the pasta phase, which exists in the inner crust of neutron stars. Alternatively, they have been combined either to phenomenological approaches through a local density approximation [13], or as an input for a density-functional approach [14]. In these approaches, adjustable parameters need, however, to be determined.

In addition to the realistic interactions, various phenomenological models have been developed, such as the Skyrme interaction [15], and have been adjusted to describe the experimental data for the ground states of finite nuclei and the empirical saturation point of symmetric nuclear matter. A simple parametrization of such phenomenological forces through the local single-particle (s.-p.) densities allows a simple solution of the Hartree-Fock (HF) equations [16]. Finally, these models have been successfully used for predictions of equations of state (EoS) of nuclear matter and description of the pasta phase within the Wigner-Seitz cell approximation [17]. In neutron stars, these models are extrapolated far from the condition where it has been adjusted and might, in some cases, become unstable [18]. The instabilities of these models could, however, be corrected such as they reproduce the features of a G matrix in nuclear matter [19].

An alternative method, which is based on realistic NN interactions and allows us to perform HF calculations similar to the phenomenological forces, is the low-momentum interaction $V_{\text{low-}k}$. The basic idea of $V_{\text{low-}k}$ is to separate the predictions for correlations at low momenta, which are constrained by the NN scattering matrix below the pion threshold, from the high-momentum components, which may strongly depend on the underlying model of realistic NN interaction. By introducing a cutoff Λ in momentum space, one separates the Hilbert space into a low-momentum and a high-momentum part. The renormalization technique (see, e.g., Refs. [20–24]) determines an effective Hamiltonian, which must be diagonalized within the model space (below the cutoff). With the cutoff in the range of $\Lambda = 2$ fm^{-1}, $V_{\text{low-}k}$ becomes model independent, and reproduces the deuteron binding energy, the low-energy phase shifts, and the half-on-shell T matrix with the same accuracy as the initial realistic interaction. This model independence demonstrates that the low-momentum physics does not depend on details of the high-momentum dynamics.

In spite of its obvious advantages, $V_{\text{low-}k}$ potential still remains a quite complicated object. On one hand, it is nonlocal and, therefore, is represented as a matrix element in momentum space for each partial-wave channel. This nonlocality increases the computational time in HF iterations, and prevents the use of $V_{\text{low-}k}$ if the number of nucleons is too large, such as in the Wigner-Seitz cells present in the crust of neutron stars,

for instance [17]. On the other hand, the renormalization technique used to produce $V_{\text{low-}k}$ seems not to be trivial. The resulting interaction is given as a matrix table, which is not an easy-to-use form and prevents this potential from being popular. A possible alternative is to find a separable representation of $V_{\text{low-}k}$, since it significantly simplifies a many-body calculation [25,26]. Moreover, recent calculations of triton-binding energies demonstrate $V_{\text{low-}k}$ can be very good approximated by a low-rank separable force for low values of the cutoff Λ [27]. We investigate the separability of $V_{\text{low-}k}$ by using the diagonalization of the matrix in momentum space for each partial-wave channel. It allows us to find a low-rank separable form of $V_{\text{low-}k}$, which can be used in HF calculations of nuclear matter as well as finite nuclei.

The $V_{\text{low-}k}$ HF calculations demonstrate a monotonic increase of the binding energy of symmetric nuclear matter as a function of the nucleon density, thus, it cannot reproduce the empirical saturation point [28,29]. Therefore, we supplement $V_{\text{low-}k}$ by a simple density-dependent contact term, which accounts for a three-body correlation. This contact term is adjusted to reproduce the saturation property of symmetric matter.

The paper is organized as follows. In Sec. II, we discuss the model space technique used to produce $V_{\text{low-}k}$ and outline the procedure to determine the separable representation. In Sec. III, we sum up all results and suggest a simple fit for the separable representation of $V_{\text{low-}k}$ as well as two different parametrizations of the contact term, adjusted for the fitted potential.

II. MODEL OF THE NN INTERACTION

The main idea of $V_{\text{low-}k}$ interaction is to disentangle the low-momentum or long-range part of a realistic NN interaction, which is fairly well described in terms of meson exchange, from the high-momentum or short-range part, where quark degrees of freedom are getting important. In other words, one defines a model space, which accounts for the low-momentum degrees of freedom and renormalizes the effective Hamiltonian for this low-momentum regime to account for the effects of the high-momentum components, which are integrated out.

In practice, the $V_{\text{low-}k}$ interaction can be derived either by using model space methods (such as Lee-Suzuki [21] or Okubo [22]) or through a renormalization-group treatment [20]. Both approaches are essentially equivalent and lead to the same energy-independent potential [23]. In the following, we will use the model space technique to disentangle these parts based on the unitary model operator approach (UMOA). This approach has frequently been described in the literature [24,28,30]. Therefore, we will restrict the presentation only to basic equations, which will define the nomenclature.

To determine the model space, the low-momentum subspace of Hilbert space, one defines a projection operator $\hat{P}$, which projects onto this model space. The complement of the subspace will be defined by the projection operator $\hat{Q}$, in such a way that the whole space is covered by these two operators. Thus, they satisfy the following relations $\hat{P} + \hat{Q} = 1$, $\hat{P}^2 = \hat{P}$, $\hat{Q}^2 = \hat{Q}$, $\hat{P}\hat{Q} = 0 = \hat{Q}\hat{P}$. The UMOA defines a unitary transformation $\hat{U}$ in such a way that the transformed Hamiltonian does not couple the $\hat{P}$ and $\hat{Q}$ spaces, that is,

$$\hat{Q}\hat{U}^{-1}\hat{H}\hat{U}\hat{P} = 0. \tag{1}$$

Now, the effective two-body interaction of Hermitian type can be determined in terms of unitary transformation $\hat{U}$ as

$$V_{\text{eff}} = V_{\text{low-}k} = \hat{U}^{-1}(\hat{h}_0 - \hat{v}_{12})\hat{U} - \hat{h}_0, \tag{2}$$

where $\hat{v}_{12}$ stands for the bare NN interaction. The operator $\hat{h}_0$ denotes the one-body part of the two-body system and contains the kinetic energy of the interacting particles. It is important to notice that, in any case, $\hat{h}_0$ commutes with the projection operators $\hat{P}$ and $\hat{Q}$. As shown by Suzuki [24], the operator $\hat{U}$ is expressed as

$$\hat{U} = (1 + \hat{\omega} - \hat{\omega}^\dagger)(1 + \hat{\omega}\hat{\omega}^\dagger + \hat{\omega}^\dagger\hat{\omega})^{-1/2}, \tag{3}$$

where an operator $\hat{\omega}$ fulfills relations $\hat{\omega} = \hat{Q}\hat{\omega}\hat{P}$ and $\hat{\omega}^2 = \hat{\omega}^{\dagger 2} = 0$. To evaluate the matrix elements of this operator $\hat{\omega}$, one should first solve the two-body eigenvalue equation,

$$(\hat{h}_0 + \hat{v}_{12})|\Phi_k\rangle = E_k|\Phi_k\rangle. \tag{4}$$

From eigenstates $|\Phi_k\rangle$, we determine those eigenstates $|\Phi_p\rangle$, which have the largest overlap with the $\hat{P}$ space. Afterwards the respective matrix elements of $\hat{\omega}$ and $\hat{U}$ may be defined in terms of $\hat{P}(\hat{Q})$ eigenstates. This matrix element of $\hat{U}$ can then be used to determine the matrix elements of the effective interaction V_{eff} in $\hat{P}$ space (for details, see Refs. [28,30]). In this manner, one obtains the effective Hamiltonian $\hat{H}_{\text{eff}} = \hat{h}_0 + \hat{V}_{\text{eff}}$. Diagonalizing it in the low-momentum model space ($\hat{P}$ space), one obtains eigenvalues, which are identical to the diagonalization of the original Hamiltonian $\hat{h}_0 + \hat{V}$ in the complete space. Moreover, the solution of the Lippmann-Schwinger equation for NN scattering phase shifts, which use $V_{\text{low-}k}$ with a cutoff Λ yields the same phase shifts as obtained from original interaction $\hat{v}_{12}$ without a cutoff. If the underlying interaction is a realistic interaction, fitted to reproduce the experimental phase shifts below Λ, these phase shifts will also be reproduced by $V_{\text{low-}k}$.

If the cutoff Λ is chosen around $\Lambda = 2$ fm^{-1}, the resulting $V_{\text{low-}k}$ is found to be essentially model independent (i.e., is independent of the underlying realistic interaction $\hat{v}_{12}$). In this sense, $V_{\text{low-}k}$ is unique and, as it reproduces the NN scattering phase shifts, it can also be regarded as a realistic interaction as, for example, the CD-Bonn [1] or Argonne V18 [2] potentials.

Originally, $V_{\text{low-}k}$ is nonlocal and is defined in terms of matrix elements on a basis of NN states labeled by relative momentum for pairs of nucleons. Thus, for each partial-wave channel, there exists a matrix, which represents $V_{\text{low-}k}(k, k')$ on a mesh of N discretized relative momenta k and k' in the range $0 \leqslant k, k' \leqslant \Lambda$. Since this matrix is real and symmetric with respect to k, k', one can diagonalize it so that it can be written as a sum of N real eigenvalues multiplied with the respective eigenvectors,

$$V_{\text{low-}k}(k, k') = \sum_{i=1}^{N} a_i f_i^*(k) f_i(k'), \tag{5}$$

where N is the number of mesh points and the dimension of the $V_{\text{low-}k}$ matrix. The eigenvectors $f_i(k)$ satisfy the orthogonality relation,

$$\frac{2}{\pi}\int_0^\Lambda dk\, k^2 f_i(k) f_j(k) = \delta_{ij}. \tag{6}$$

In the following, we will omit the symbol of complex conjugation because all eigenvectors are real. The last equality Eq. (5) is nothing else but the general definition of a separable potential of the rank N. If the rank of the separable potential equals the dimension of the matrix $V_{\text{low-}k}(k, k')$, all information is exactly restored from the eigenvalues a_i and eigenvectors f_i. As we will see later, some eigenvalues a_i can be zero or negligibly small so that one can reduce the rank of the separable interaction by taking only the n eigenvalues with the largest absolute values into account. It leads to a new approximated separable interaction $V^{[n]}_{\text{low-}k}(k, k')$:

$$V_{\text{low-}k}(k, k') \simeq V^{[n]}_{\text{low-}k}(k, k') = \sum_{i=1}^{n} a_i f_i(k) f_i(k'), \quad (n \leqslant N). \tag{7}$$

The low-rank separable representation of the NN interaction leads to significant simplifications in many-body calculations.

The effective interaction $V_{\text{low-}k}$ as well as its separable form is nonlocal and is defined in terms of matrix elements in momentum space. It implies that the HF calculations have to be performed in a Hilbert space by using an appropriate basis $|\alpha\rangle, |\beta\rangle, \ldots$. The HF Hamiltonian is then expressed in terms of the matrix elements between these basis states $\langle\alpha|H_{\text{HF}}|\beta\rangle$, and the HF s.-p. states $|\Psi_n\rangle$ are expressed through the expansion coefficients on the basis,

$$|\Psi_n\rangle = \sum_\alpha |\alpha\rangle\langle\alpha|\Psi_n\rangle = \sum_\alpha c_{n\alpha}|\alpha\rangle. \tag{8}$$

The part of the HF Hamiltonian, which originates from $V_{\text{low-}k}$, can be expressed in terms of two-body matrix elements by

$$\langle\alpha|H_{\text{low-}k}|\beta\rangle = \sum_{\gamma,\delta}\langle\alpha\gamma|V_{\text{low-}k}|\beta\delta\rangle\rho_{\gamma\delta}, \tag{9}$$

where $\rho_{\gamma\delta}$ is the s.-p. density matrix. To investigate the bulk properties of finite nuclei, we perform HF calculations within the spherical Wigner-Seitz cell by assuming a plane-wave s.-p. basis [31,32].

III. RESULTS AND DISCUSSION

In the following, we discuss results for symmetric nuclear matter as well as finite nuclei obtained from HF calculations. These calculations are performed in the model space, which is defined by a cutoff parameter Λ in the two-body scattering equation, which employs the corresponding low-momentum interaction $V_{\text{low-}k}$, which is derived from the CD-Bonn [1] interaction by using the technique described in Sec. II. The NN interaction has been restricted to partial waves with total angular momentum $J \leqslant 6$.

We start our discussion with the comparison of the eigenvalues a_i obtained from diagonalization of a 20×20 matrix of $V_{\text{low-}k}(k, k')$ in the $^1S_0$ channel. The resulting nonzero eigenvalues are shown in the top panel of Fig. 1 for different values of Λ. As discussed previously, $V_{\text{low-}k}$ interaction becomes model independent at $\Lambda = 2$ fm^{-1}. At this value of the cutoff parameter Λ, the diagonalization procedure yields only 11 nonzero eigenvalues, in other words, $V_{\text{low-}k}$ interaction in the $^1S_0$ channel is a separable interaction of the 11th rank or, by following Eq. (5), one can write

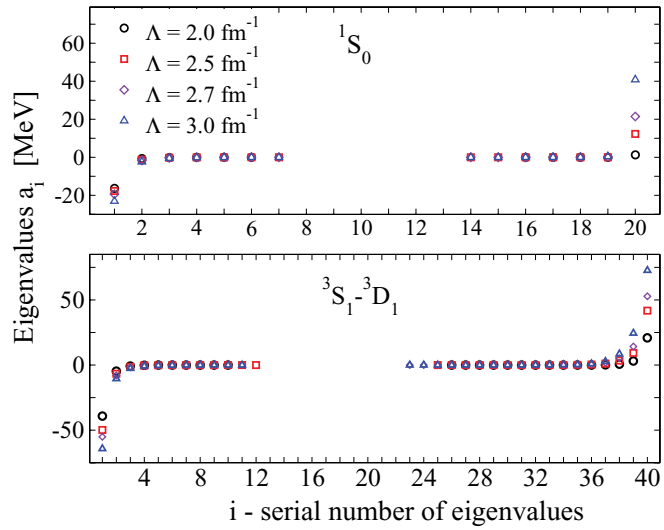

FIG. 1. (Color online) Top: Nonzero eigenvalues a_i of the $^1S_0$ channel. Bottom: Nonzero eigenvalues a_i of the $^3S_1$-$^3D_1$ channel.

$$V^{[11]}_{\text{low-}k}(k, k') = V_{\text{low-}k}(k, k'). \tag{10}$$

The nonzero eigenvalues are essentially independent of N, the dimension of the matrix, which represents $V_{\text{low-}k}$. Furthermore, one can notice that many of the nonzero eigenvalues are, nevertheless, very small, and only some of them (e.g., at $i = 1, 2, 20$) carry the main piece of information about the interaction model. This gives rise to a substantial lowering of the rank of the separable potential, as shown in Eq. (7). With the increase of the cutoff Λ, the absolute values of the eigenvalues increase as well; and, as a consequence, the rank n of the separable form $V^{[n]}_{\text{low-}k}$ defined in Eq. (7) has to be increased to achieve reasonable accuracy. By increasing Λ, more information about the short-range components of the underlying bare interaction is included, which requires a larger rank in the separable representation of the interaction. This is in line with the findings of Bogner *et al.* [33] who explored the finite-rank expansion of the low-momentum interaction by means of a Weinberg eigenvalue analysis.

In the case of the coupled channels, such as the $^3S_1$-$^3D_1$ channel, the dimension N of the $V_{\text{low-}k}$ matrix is twice as large if one keeps the number of mesh points in each channel the same as for the uncoupled partial waves. It turns out that the number of nonzero eigenvalues also increases as shown in the lower panel of Fig. 1. It is obvious that the rank of the separable potential should be higher than for the $^1S_0$ channel. It is a general feature that coupled channels require higher rank separable interaction than the uncoupled ones [34]. Also, one observes pairs of positive and negative eigenvalues, which

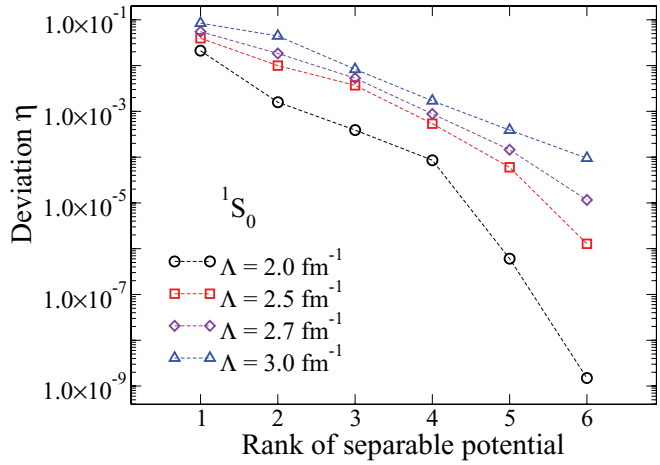

FIG. 2. (Color online) Squared deviation of the separable $V^{[n]}_{\text{low-}k}(k,k')$ from the original $V_{\text{low-}k}(k,k')$ in the $^1S_0$ channel for different values of the cutoff parameter Λ.

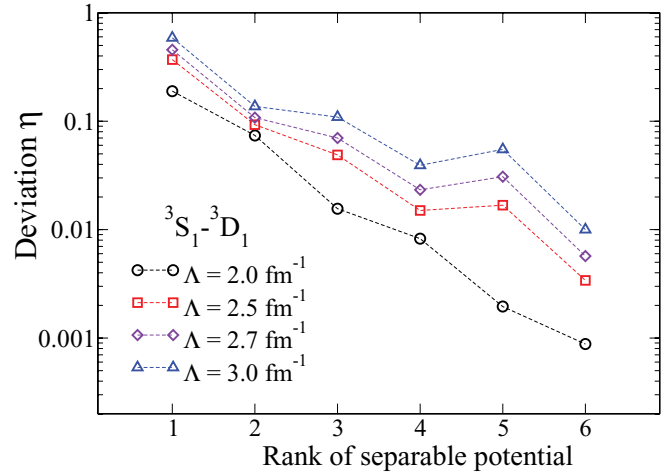

FIG. 3. (Color online) Squared deviation of the separable $V^{[n]}_{\text{low-}k}(k,k')$ from the original $V_{\text{low-}k}(k,k')$ in the $^3S_1$-$^3D_1$ channel for different values of the cutoff parameter Λ.

have about the same absolute value. This picture remains for higher values of Λ. As we will see later, this symmetry between positive and negative eigenvalues will play a crucial role in the convergence of the separable form $V^{[n]}_{\text{low-}k}$ to the initial $V_{\text{low-}k}$ with an increase in rank.

To determine a minimal rank for a reliable separable approximation in each channel, we calculate the square deviation η of the separable form $V^{[n]}_{\text{low-}k}$ from the original potential $V_{\text{low-}k}$ for each rank n:

$$\eta = \sum_{k,k'} \left| V_{\text{low-}k}(k,k') - V^{[n]}_{\text{low-}k}(k,k') \right|^2 \Big/ \sum_{k,k'} |V_{\text{low-}k}(k,k')|^2. \tag{11}$$

In Fig. 2, the deviation for the $^1S_0$ channel at different values of the cutoff Λ is shown. At $\Lambda = 2$ fm^{-1}, one observes a fast convergence to zero deviation already at the rank $n = 2$. The growth of the cutoff monotonically increases the rank of the separable potential. At $\Lambda = 3$ fm^{-1}, one may expect good accuracy starting from $n = 5$.

The deviation η for the $^3S_1$-$^3D_1$ channel is displayed in Fig. 3. First, at low n, the absolute value of the deviation is 1 order of magnitude higher than for the uncoupled $^1S_0$ channel. By increasing the rank, one observes a nonmonotonic oscillating decrease of η, specially for high Λ. As we have seen, the diagonalization of the channel $^3S_1$-$^3D_1$ yields both positive and negative eigenvalues, which are symmetrically distributed over i so that they form pairs with very similar absolute values. By assuming the odd rank, we take either the uncompensated positive or the negative eigenvalue into account. This eigenvalue will be compensated in the next (even) rank, and accuracy will be significantly improved.

The deviation η for other channels at $\Lambda = 2$ fm^{-1} is shown in Figs. 4 and 5. In the following, we choose the second rank approximation for the uncoupled channels ($n = 2$) and the third rank for the coupled one ($n = 3$). In the following, the respective separable version of $V_{\text{low-}k}$ will be referred to as $V^{[2,3]}_{\text{low-}k}$.

Now, let us turn to the binding energy of symmetric nuclear matter, which is displayed in Fig. 6. The HF calculations, which use $V^{[2,3]}_{\text{low-}k}$ (dashed line), essentially yield the same result as the one that employs the original $V_{\text{low-}k}$ interaction (solid curve). The deviation does not exceed 1% at the saturation density ρ_0 and 1.7% at the density $2\rho_0$. We also compared the binding energy of pure neutron matter for both potentials and found that the discrepancy is less than 1% for the same range of densities.

However, neither of the two calculations yields a saturation point (i.e., a minimum in the energy versus the density plot), as was observed before [29,35]. This absence of saturation is one of the main problems in calculations of nuclear matter, which employ $V_{\text{low-}k}$. It cannot be cured by the inclusion of correlations beyond the HF approximation (e.g., by means of the Brueckner-Hartree-Fock approximation [28]). Recent relativistic calculations by van Dalen and Müther demonstrate that saturation can be achieved within the $V_{\text{low-}k}$ approach by inclusion of relativistic effects in dressing the Dirac spinors,

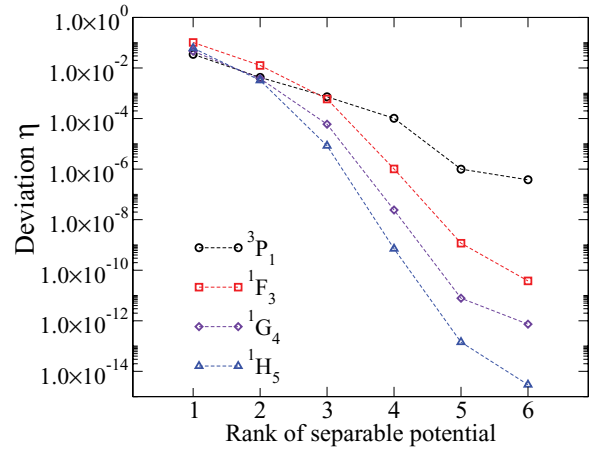

FIG. 4. (Color online) Squared deviation of the separable $V^{[n]}_{\text{low-}k}(k,k')$ from the original $V_{\text{low-}k}(k,k')$ for various uncoupled channels at $\Lambda = 2$ fm^{-1}.

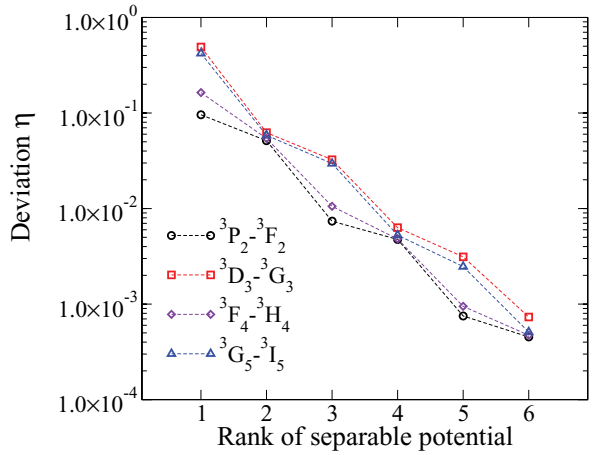

FIG. 5. (Color online) Squared deviation of the separable $V^{[n]}_{\text{low-}k}(k,k')$ from the original $V_{\text{low-}k}(k,k')$ for various coupled channels at $\Lambda = 2$ fm^{-1}.

which are used to evaluate the underlying realistic interaction [36].

All results obtained so far indicate that $V^{[2,3]}_{\text{low-}k}$ is an accurate low-rank separable representation of $V_{\text{low-}k}$ interaction. However, to make it accessible to other users, it should be parametrized in a simple form. Here, we suggest the fitting function for all $f_i(k)$ in all channels,

$$f_i(k) = \alpha_i + [\beta_i \exp(\gamma_i k^{\delta_i}) + \mu_i] \sin(k\sigma_i + \lambda_i), \qquad (12)$$

which contains seven parameters for each partial-wave channel and each $f_i(k)$. In Table I, we summarized all parameters of the separable fitted form for uncoupled channels, while all parameters for the coupled channels are shown in Table II. By using the values from both tables, one can reproduce the fitted version of $V^{[2,3]}_{\text{low-}k}$ for a given partial-wave channel. In the following, we will identify the respective separable fitted potential as $V^{[2,3]}_{\text{fit}}$.

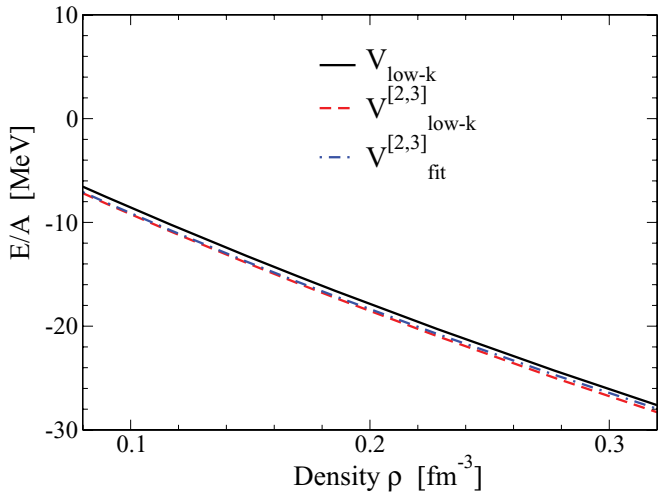

FIG. 6. (Color online) Energy per nucleon of symmetric nuclear matter as a function of the density. Results of the $V_{\text{low-}k}$ interaction (solid line) compared with the separable form $V^{[2,3]}_{\text{low-}k}$ (dashed line) and the respective fitted form $V^{[2,3]}_{\text{fit}}$ (dashed-dotted line).

To check the accuracy of our fit, we perform HF calculations of nuclear matter that employ $V^{[2,3]}_{\text{fit}}$. The respective binding energy as a function of the density of symmetric nuclear matter is displayed in Fig. 6 by a dashed-dotted line. One observes that, at up to saturation density $\rho_0 \simeq 0.16$ fm^{-3}, the fitted potential $V^{[2,3]}_{\text{fit}}$ reproduces the results of $V^{[2,3]}_{\text{low-}k}$ (red dashed), while at higher densities, it becomes slightly less bound and lies closer to the original $V_{\text{low-}k}$ (solid). Thus, the deviation of the fitted separable potential $V^{[2,3]}_{\text{fit}}$ from $V_{\text{low-}k}$ does not exceed 1% of the binding energy. By not going into detail, we mention that the deviation rises mainly from the $^3S_1$-$^3D_1$ and the $^3P_2$-$^3F_2$ coupled channels.

As we have already seen from Fig. 6, $V_{\text{low-}k}$ interaction as well as its separable form $V^{[2,3]}_{\text{fit}}$ does not describe the empirical saturation point. To achieve the saturation in nuclear matter, one has to add three-body interaction terms or a density-dependent two-nucleon interaction. Therefore, we support the low-momentum interaction by a simple contact interaction, which has been chosen by following the notation of the Skyrme interaction [15,16],

$$\Delta v = \Delta v_0 + \Delta v_3, \qquad (13)$$

with

$$\Delta v_0 = \tfrac{1}{4} t_0 \big[(2+x_0)\rho^2 - (2x_0+1)\big(\rho_n^2 + \rho_p^2\big)\big], \qquad (14)$$

and

$$\Delta v_3 = \tfrac{1}{24} t_3 \rho^\alpha \big[(2+x_3)\rho^2 - (2x_3+1)\big(\rho_n^2 + \rho_p^2\big)\big], \qquad (15)$$

where ρ_p and ρ_n are the local densities of nucleons, while the total matter density is denoted as $\rho = \rho_p + \rho_n$. The values of α and x_0 were fixed at $\alpha = 0.5$, $x_0 = 0.0$, while t_0, t_3, and x_3 were fitted in such a way that HF calculations that use $V_{\text{low-}k}$ or $V^{[2,3]}_{\text{fit}}$ plus the contact term of Eq. (13) reproduce both the empirical saturation point of the symmetric nuclear matter and the symmetry energy at saturation density. By following Ref. [32], the contact interaction produced for $V_{\text{low-}k}$ will be labeled by CT, and the respective interaction model will be labeled $V_{\text{low-}k} + \text{CT}$. For the fitted potential $V^{[2,3]}_{\text{fit}}$, we suggest

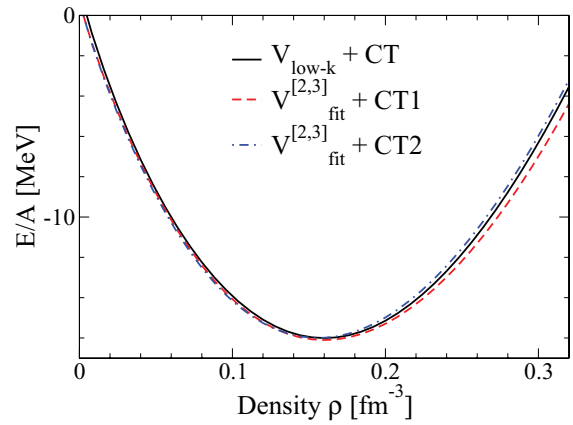

FIG. 7. (Color online) Energy per nucleon of symmetric nuclear matter as a function of the density. Results of $V_{\text{low-}k} + \text{CT}$ interaction (solid line) compared with the fitted separable form $V^{[2,3]}_{\text{fit}} + \text{CT1}$ (dashed line) and $V^{[2,3]}_{\text{fit}} + \text{CT2}$ (dashed-dotted line).

TABLE I. Parameters of $V_{\text{fit}}^{[2,3]}$ for uncoupled channels. See Eq. (12).

Channel	i	a_i	α_i	β_i	γ_i	δ_i	μ_i	σ_i	λ_i
$^1S_0$	1	$-0.163\,44 \times 10^2$	$0.107\,72 \times 10^{-3}$	$-0.432\,34 \times 10^{-3}$	0.1765	0.9261	$0.103\,16 \times 10^{-2}$	0.993 35	1.4191
	2	−0.6677	$-0.207\,49 \times 10^{-3}$	−0.018 295	0.066 232	0.868 15	0.020 236	1.7925	1.1085
$^1P_1$	1	$0.145\,69 \times 10^2$	$-0.360\,52 \times 10^{-2}$	0.1238×10^{-2}	0.300 93	1.572	$0.240\,98 \times 10^{-2}$	0.469 96	1.4196
	2	1.5105	$0.411\,03 \times 10^{-4}$	$-0.300\,56 \times 10^{-2}$	0.046 402	1.2591	$0.366\,18 \times 10^{-2}$	2.2676	$-0.662\,86 \times 10^{-2}$
$^3P_0$	1	3.6518	$0.349\,15 \times 10^{-4}$	$-0.391\,91 \times 10^{-3}$	0.074 648	3.5155	$0.357\,79 \times 10^{-3}$	2.0292	1.4199
	2	−3.6339	$0.122\,54 \times 10^{-3}$	$0.209\,82 \times 10^{-3}$	−0.598 88	1.0769	$0.303\,73 \times 10^{-3}$	−2.1878	9.6652
$^3P_1$	1	0.1541×10^2	$-0.335\,98 \times 10^{-3}$	$0.151\,82 \times 10^{-2}$	$-0.127\,01 \times 10^{-2}$	5.4199	-0.8545×10^{-3}	0.5981	0.527 99
	2	1.1011	$-0.444\,21 \times 10^{-3}$	$0.188\,96 \times 10^{-2}$	−0.631 58	2.4471	$0.945\,46 \times 10^{-4}$	0.734 98	0.225 58
$^1D_2$	1	−4.7228	$0.239\,48 \times 10^{-3}$	$0.115\,14 \times 10^{-2}$	0.078 532	0.8308	$-0.140\,43 \times 10^{-2}$	1.5502	1.2639
	2	−0.4272	$0.432\,76 \times 10^{-3}$	$-0.133\,08 \times 10^{-2}$	−0.761 08	2.2797	$0.892\,15 \times 10^{-3}$	1.281	1.7046
$^3D_2$	1	$-0.147\,55 \times 10^2$	$0.236\,61 \times 10^{-3}$	$-0.162\,14 \times 10^{-3}$	−0.200 28	4.7727	$-0.796\,36 \times 10^{-4}$	1.2915	1.7118
	2	−2.0625	$0.468\,73 \times 10^{-3}$	$-0.132\,99 \times 10^{-2}$	−0.707 97	2.2075	$0.858\,42 \times 10^{-3}$	1.4395	1.6497
$^1F_3$	1	2.1276	$0.116\,82 \times 10^{-3}$	$-0.248\,64 \times 10^{-3}$	−1.5328	−0.761 12	$-0.117\,25 \times 10^{-3}$	2.0029	1.4366
	2	0.4558	$0.454\,34 \times 10^{-3}$	$0.342\,63 \times 10^{-2}$	−2.3846	−1.2925	$-0.455\,76 \times 10^{-3}$	1.8623	1.4425
$^3F_3$	1	1.1895	$0.128\,11 \times 10^{-3}$	$-0.895\,37 \times 10^{-4}$	−0.631 86	−1.3835	$-0.128\,93 \times 10^{-3}$	2.096	1.3909
	2	0.2674	$0.440\,76 \times 10^{-3}$	$0.353\,97 \times 10^{-2}$	−2.4171	−1.2481	$-0.442\,04 \times 10^{-3}$	1.8298	1.45
$^1G_4$	1	−0.567 13	$0.935\,11 \times 10^{-4}$	$-0.326\,73 \times 10^{-3}$	−1.4289	−1.0215	$-0.946\,13 \times 10^{-4}$	1.9148	1.3505
	2	−0.091 76	$0.922\,67 \times 10^{-2}$	−0.014 963	−5.566	−1.8735	$-0.923\,35 \times 10^{-2}$	−0.378 57	1.6284
$^3G_4$	1	−3.027	$0.107\,74 \times 10^{-3}$	$-0.161\,21 \times 10^{-3}$	−0.7781	−1.5648	-0.1094×10^{-3}	1.8745	1.3214
	2	−0.5061	$0.101\,91 \times 10^{-3}$	$-0.620\,66 \times 10^{-3}$	−1.0817	−1.0648	$-0.103\,92 \times 10^{-3}$	3.1194	1.3385
$^1H_5$	1	0.6095	$0.144\,58 \times 10^{-6}$	$-0.434\,67 \times 10^{-3}$	−0.304 81	3.4986	$0.435\,36 \times 10^{-3}$	1.3486	−0.296 05
	2	0.1455	$0.998\,49 \times 10^{-4}$	$-0.381\,55 \times 10^{-3}$	−0.646 24	−2.4138	$-0.108\,03 \times 10^{-3}$	3.3677	0.959 75
$^3H_5$	1	0.3736	$0.172\,06 \times 10^{-6}$	$-0.456\,36 \times 10^{-3}$	−0.288 89	3.4083	$0.457\,08 \times 10^{-3}$	1.378	−0.3199
	2	0.007 27	$0.867\,39 \times 10^{-4}$	$-0.361\,73 \times 10^{-3}$	−0.886 87	2.9817	$0.451\,15 \times 10^{-3}$	3.2408	−2.0198
$^1I_6$	1	−0.1407	$0.186\,15 \times 10^{-4}$	-0.2782×10^{-4}	1.5265	0.972 82	$0.152\,76 \times 10^{-4}$	2.0513	1.5767
	2	−0.0281	0.635 51	−0.267 03	0.187 34	1.9309	−0.367 58	0.398 62	1.576
$^3I_6$	1	−0.8297	$-0.187\,13 \times 10^{-4}$	−0.306 95	$0.313\,41 \times 10^{-3}$	2.1961	0.306 94	1.9374	1.6207
	2	−0.153	0.9446×10^{-4}	−0.3064	$0.531\,29 \times 10^{-3}$	1.4854	0.3063	3.3132	7.9134

TABLE II. Parameters of $V_{\rm fit}^{[2,3]}$ for coupled channels. See Eq. (12).

Channel	i	a_i	α_i	β_i	γ_i	δ_i	μ_i	σ_i	λ_i
$^3S_1$	1	$-0.391\,95 \times 10^2$	0.1471×10^{-3}	$-0.278\,82 \times 10^{-2}$	0.101 66	0.987 61	$0.331\,48 \times 10^{-2}$	0.734 93	0.917 75
	2	$0.209\,13 \times 10^2$	$-0.975\,62 \times 10^{-4}$	0.332 92	$0.506\,09 \times 10^{-3}$	0.877 32	−0.333 39	1.4274	1.2444
	3	−4.6417	$-0.218\,67 \times 10^{-4}$	0.312 58	$0.175\,66 \times 10^{-2}$	0.787 84	−0.313 68	1.8855	1.1761
$^3D_1$	1	$-0.391\,95 \times 10^2$	$0.901\,22 \times 10^{-4}$	$0.313\,69 \times 10^{-5}$	$0.389\,17 \times 10^{-3}$	$0.124\,44 \times 10^2$	$-0.931\,23 \times 10^{-4}$	1.3384	1.5561
	2	$0.209\,13 \times 10^2$	$0.112\,07 \times 10^{-3}$	$-0.137\,05 \times 10^{-4}$	0.482 96	2.4592	$-0.978\,61 \times 10^{-4}$	2.1818	1.5329
	3	−4.6417	$-0.226\,45 \times 10^{-3}$	−0.412 35	$0.409\,73 \times 10^{-3}$	1.8283	0.412 58	1.5668	1.5335
$^3P_2$	1	$-0.117\,12 \times 10^2$	−0.012 771	$0.749\,67 \times 10^{-2}$	0.029 157	0.837 36	$0.530\,84 \times 10^{-2}$	0.119 92	1.4904
	2	−2.1898	$-0.921\,01 \times 10^{-4}$	0.282 19	$0.195\,54 \times 10^{-2}$	1.198	−0.282 96	1.2014	−0.127 09
	3	1.7808	$0.140\,09 \times 10^{-3}$	0.346 22	$0.137\,19 \times 10^{-2}$	1.2162	−0.346 94	1.2159	2.9393
$^3F_2$	1	$-0.117\,12 \times 10^2$	$-0.379\,75 \times 10^{-5}$	$-0.267\,53 \times 10^{-9}$	$0.118\,62 \times 10^2$	0.1152	$-0.690\,54 \times 10^{-5}$	1.0568	−0.531 09
	2	−2.1898	$0.715\,89 \times 10^{-4}$	$-0.984\,97 \times 10^{-14}$	$0.224\,38 \times 10^2$	0.054 423	$-0.693\,08 \times 10^{-4}$	−2.3032	−4.6525
	3	1.7808	$0.247\,33 \times 10^{-3}$	$-0.693\,63 \times 10^{-4}$	1.2429	0.450 15	$0.404\,33 \times 10^{-3}$	1.1919	4.0019
$^3D_3$	1	−6.0466	$0.183\,32 \times 10^{-3}$	0.142 66	$0.414\,43 \times 10^{-3}$	1.7445	−0.142 84	2.1656	1.5038
	2	5.4641	$-0.273\,73 \times 10^{-3}$	−0.456 81	$0.679\,93 \times 10^{-3}$	0.909 16	0.457 13	1.8906	0.9951
	3	0.9141	$-0.116\,06 \times 10^{-3}$	0.181 14	−0.132 13	0.1251×10^{-2}	−0.159 01	3.3728	−0.796 66
$^3G_3$	1	−6.0466	$0.419\,21 \times 10^{-4}$	−0.065 759	$0.793\,78 \times 10^{-3}$	1.8207	0.065 717	1.424	1.675
	2	5.4641	$0.158\,08 \times 10^{-3}$	$-0.164\,19 \times 10^{-3}$	−0.103 45	−0.994 77	$0.289\,59 \times 10^{-3}$	1.9522	−2.5907
	3	0.9141	$0.788\,27 \times 10^{-4}$	−0.073 989	$-0.173\,82 \times 10^{-2}$	1.5332	0.074 065	3.0794	−1.8745
$^3F_4$	1	−1.6095	$0.180\,33 \times 10^{-3}$	0.378 79	$-0.394\,28 \times 10^{-3}$	0.3739	−0.378 52	2.1928	−2.339
	2	0.5616	$0.241\,68 \times 10^{-3}$	−1.1138	$-0.808\,23 \times 10^{-4}$	2.7458	1.1135	1.9919	1.3089
	3	−0.3036	$-0.320\,58 \times 10^{-3}$	−1.1873	$0.289\,72 \times 10^{-3}$	1.6371	1.1877	2.0173	1.1166
$^3H_4$	1	−1.6095	$0.304\,49 \times 10^{-7}$	0.028 581	−6.9621	−0.544 67	$0.150\,57 \times 10^{-5}$	1.0041	3.0546
	2	0.5616	$0.175\,31 \times 10^{-4}$	0.223 51	$0.341\,14 \times 10^{-3}$	1.9278	−0.223 49	1.6346	−1.2499
	3	−0.3036	-0.1491×10^{-2}	0.2092	$0.260\,23 \times 10^{-2}$	2.44	−0.2077	0.592 66	1.638
$^3G_5$	1	1.6137	$-0.935\,23 \times 10^{-4}$	−0.489 52	-0.8851×10^{-4}	1.0928	0.489 61	2.5801	1.1545
	2	−1.2501	$0.131\,11 \times 10^{-3}$	−0.135 21	−0.107 57	$0.101\,62 \times 10^{-2}$	0.1213	2.8269	0.7056
	3	0.3088	$-0.318\,41 \times 10^{-3}$	−0.535 98	$0.612\,43 \times 10^{-3}$	1.8397	0.536 33	2.3654	0.991 54
$^3I_5$	1	1.6137	$0.140\,23 \times 10^{-4}$	0.367 54	$-0.140\,39 \times 10^{-3}$	2.588	−0.367 55	1.7978	1.5991
	$2s$	−1.2501	$0.191\,69 \times 10^{-4}$	0.295 12	$0.154\,69 \times 10^{-3}$	2.6251	−0.2951	1.7038	−1.6316
	3	0.3088	$0.388\,21 \times 10^{-4}$	0.361 56	$0.350\,17 \times 10^{-3}$	1.9665	−0.361 53	3.0449	−2.1756
$^3H_6$	1	−0.3054	$-0.654\,38 \times 10^{-3}$	0.651 43	$0.560\,31 \times 10^{-3}$	2.3634	−0.650 75	0.487 47	1.8318
	2	0.2096	$0.613\,33 \times 10^{-4}$	0.259 66	$-0.328\,93 \times 10^{-3}$	1.3102	−0.259 72	2.5754	1.1963
	3	−0.0637	$0.256\,01 \times 10^{-3}$	0.398 08	$0.292\,43 \times 10^{-3}$	3.2313	−0.398 36	2.2583	1.0325
$^3K_6$	1	−0.3054	$-0.102\,69 \times 10^{-4}$	0.235 04	$0.147\,85 \times 10^{-3}$	3.1131	−0.235 03	1.8245	1.4457
	2	0.2096	$0.120\,93 \times 10^{-4}$	−0.367 99	$0.114\,73 \times 10^{-3}$	3.0036	0.367 98	1.806	1.4804
	3	−0.0637	$-0.196\,63 \times 10^{-4}$	0.263 22	$0.393\,36 \times 10^{-3}$	2.3907	−0.2632	2.9488	0.913 09

TABLE III. Parameters of the contact interaction defined in Eq. (13). The set CT was produced for $V_{\text{low-}k}$ [32], while CT1 and CT2 supply $V_{\text{fit}}^{[2,3]}$.

Interaction	t_0 (MeV fm^3)	t_3 (MeV fm$^{3+3\alpha}$)	x_3
CT	−584.1	8330.7	−0.5
CT1	−548.0	7890.13	−0.5
CT2	−565.467	8180.0	−0.5

two possible parametrizations: CT1 and CT2. Their parameters and properties of nuclear matter are shown in Tables III and IV, respectively. The interaction $V_{\text{fit}}^{[2,3]}$ + CT1 gives the binding energy per nucleon of symmetric nuclear matter $E/A = -16.1$ MeV at the density $\rho_0 = 0.16$ fm^{-3}. The HF calculations of nuclear matter (see Fig. 7) for $V_{\text{fit}}^{[2,3]}$ + CT1 give results (dashed line) very similar to the nonseparable initial interaction $V_{\text{low-}k}$ + CT (solid line). However, in the calculation of finite nuclei, we observe a deviation of about 0.12 MeV in the binding energy of light nuclei, such as ^{16}O (see Table V). The picture can be improved if we assume that the saturation density is not defined exactly and allow for a small deviation. Along this line, the second parametrization CT2 was produced. The interaction $V_{\text{fit}}^{[2,3]}$ + CT2 gives $E/A = -16.0$ MeV at the density $\rho_0 = 0.156$ fm^{-3}. This corresponds to a small shift of the saturation point with respect to the initial $V_{\text{low-k}}$ interaction (see Fig. 7). It allows us to improve the accuracy in the binding energies of finite nuclei: One can notice that the contact interaction CT2 leads to a better description than CT1. However, by comparing the rms charge radii of nuclei in Table V, we see that, due to the shift in saturation density, the interaction $V_{\text{fit}}^{[2,3]}$ + CT2 yields larger radii than the interaction $V_{\text{fit}}^{[2,3]}$ + CT1.

For all models considered here, the compressibility modulus at saturation density is in the range $240.5 \leqslant K \leqslant 258$ MeV. This means that the respective EoS displayed in Fig. 7 are rather soft, at least at densities up to about two times the saturation density. Such a prediction of a soft EoS is in agreement with data extracted from heavy-ion reactions. For example, heavy-ion data for transverse flow [41] or from kaon production [42] support the picture of a soft EoS in symmetric nuclear matter. This value for the compressibility modulus is also in agreement with that of the Skyrme interaction, which correctly reproduces the breathing mode in nuclei (giant isoscalar resonance) [43].

It is interesting to notice that the accuracy obtained with our semiempirical models for the comparison of binding energies and radii of representative nuclei (cf. Table V) is comparable

TABLE IV. Bulk properties of symmetric nuclear matter derived from $V_{\text{low-}k}$ and its separable representation. They are supplemented by the respective contact interaction.

Interaction	ρ_0 (fm^{-3})	$E/A(\rho_0)$ (MeV)	K (MeV)
$V_{\text{low-}k}$ + CT	0.16	−16.0	258
$V_{\text{fit}}^{[2,3]}$ + CT1	0.16	−16.1	241.9
$V_{\text{fit}}^{[2,3]}$ + CT2	0.156	−16.0	240.5

TABLE V. The binding energy per nucleon and rms charge radii of finite nuclei. Experimental data taken from Refs. [37–40].

Interaction	^{16}O	^{40}Ca	^{48}Ca	^{60}Ca	^{208}Pb
		E/A (MeV)			
$V_{\text{low-}k}$ + CT	−7.91	−8.57	−8.42	−7.75	−7.76
$V_{\text{fit}}^{[2,3]}$ + CT1	−7.79	−8.56	−8.35	−7.78	−7.76
$V_{\text{fit}}^{[2,3]}$ + CT2	−7.84	−8.58	−8.37	−7.79	−7.76
Experiment	−7.98	−8.55	−8.67	–	−7.87
		r_{ch} (fm)			
$V_{\text{low-}k}$ + CT	2.79	3.50	3.54	3.68	5.51
$V_{\text{fit}}^{[2,3]}$ + CT1	2.81	3.51	3.55	3.68	5.52
$V_{\text{fit}}^{[2,3]}$ + CT2	2.82	3.53	3.58	3.71	5.56
Experiment	2.74	3.48	3.47	–	5.50

to that of the widely used Skyrme interactions, such as SLy4, for instance, while the number of free parameters is only 3 (t_0, t_3, x_3). The number of empirical data needed to adjust the interaction is, therefore, reduced compared to empirical nuclear interactions; and the interaction model we propose contains interesting features of the complex bare potential such as, for instance, the tensor matrix elements. Studies of $T = 0$ and $T = 1$ pairing channels as well as the properties of exotic nuclei will be addressed in future applications of our model.

IV. SUMMARY AND CONCLUSION

In the past decade, it has become popular to perform nuclear structure calculations by using the low-momentum NN interaction $V_{\text{low-}k}$ (see, for instance, the recent Refs. [44,45]). This interaction is constructed from a realistic NN interaction by introducing a cutoff Λ in the relative momenta of the interacting nucleons. We used a model space technique on the basis of the unitary model operator approach to separate the low-momentum and the high-momentum parts of the initial CD-Bonn interaction. The cutoff parameter Λ was fixed at $\Lambda = 2$ fm^{-1} so that a $V_{\text{low-}k}$ was obtained, which was essentially independent of the underlying bare NN interaction.

The resulting $V_{\text{low-}k}$ interaction is nonlocal and is defined in terms of matrix elements in momentum space for each partial-wave channel. This allows us to use a diagonalization method to express the matrix elements in a separable form. We investigate the separability in different channels with an increase of the cutoff Λ. It was found that, at $\Lambda = 2$ fm^{-1}, the low-momentum interaction can accurately be approximated by a low-rank separable interaction. This separable interaction is parametrized to make it accessible for other nuclear structure calculations.

A density-dependent contact interaction is added to reproduce the saturation property of the infinite nuclear matter. HF calculations, which use this interaction model, also reproduce the bulk properties of finite nuclei with good accuracy. Therefore, we are able to define an effective interaction, which is based on a realistic NN interaction, reproduces the bulk properties of nuclear matter as well as finite nuclei, and is easy to use. In contrast to effective interactions, which

originate from a pure phenomenological approach such as, for example, the various versions of the Skyrme interaction, this interaction model should also be valid for nuclei far away from the valley of stability and approaches going beyond the HF approximation and accounts for pairing or more complex correlations [46].

This work has been supported by the European Graduate School Hadrons in Vacuum, in Nuclei and Stars (Basel, Graz, Tübingen) and Grant No. Mu 705/5-2 of the Deutsche Forschungsgemeinschaft (DFG) and by CompStar, a Research Networking Programme of the European Science Foundation.

[1] R. Machleidt, F. Sammarruca, and Y. Song, Phys. Rev. C **53**, R1483 (1996).
[2] R. B. Wiringa, V. G. J. Stoks, and R. Schiavilla, Phys. Rev. C **51**, 38 (1995).
[3] V. G. J. Stoks, R. A. M. Klomp, C. P. F. Terheggen, and J. J. de Swart, Phys. Rev. C **49**, 2950 (1994).
[4] D. R. Entem and R. Machleidt, Phys. Rev. C **68**, 041001(R) (2003).
[5] M. Baldo, in *Nuclear Methods and the Nuclear Equation of State*, edited by M. Baldo (World Scientific, Singapore, 1999).
[6] E. Feenberg, *Theory of Quantum Fluids* (Academic, New York, 1969).
[7] R. B. Wiringa, S. C. Pieper, J. Carlson, and V. R. Pandharipande, Phys. Rev. C **62**, 014001 (2000).
[8] W. H. Dickhoff and D. Van Neck, *Many-Body Theory Exposed!* (World Scientific, Singapore, 2005).
[9] P. Gögelein, E. N. E. van Dalen, K. Gad, K. S. A. Hassaneen, and H. Müther, Phys. Rev. C **79**, 024308 (2009).
[10] A. Fabrocini, S. Fantoni, A. Y. Illarionov, and K. E. Schmidt, Nucl. Phys. A **803**, 137 (2008).
[11] N. Farina, Ph.D. thesis, Universita di Roma, 2008.
[12] O. Benhar and A. Carbonne, arXiv:0912.0129 [nucl-th].
[13] M. Baldo, U. Lombardo, É. E. Saperstein, and S. V. Tolokonnikov, JETP Lett. **80**, 523 (2004).
[14] M. Baldo, P. Schuck, and X. Viñas, Phys. Lett. B **663**, 390 (2008).
[15] T. H. R. Skyrme, Nucl. Phys. **9**, 615 (1959).
[16] D. Vautherin and D. M. Brink, Phys. Rev. C **5**, 626 (1972).
[17] J. W. Negele and D. Vautherin, Nucl. Phys. A **207**, 298 (1973).
[18] J. Margueron, J. Navarro, and N. Van Giai, Phys. Rev. C **66**, 014303 (2002).
[19] J. Margueron and H. Sagawa, J. Phys. G **36**, 125102 (2009).
[20] S. K. Bogner, T. T. S. Kuo, and L. Coraggio, Nucl. Phys. A **684**, 432c (2001).
[21] S. Y. Lee and K. Suzuki, Phys. Lett. B **91**, 173 (1980).
[22] S. Okubo, Prog. Theor. Phys. **12**, 603 (1954).
[23] S. K. Bogner, R. J. Furnstahl, and A. Schwenk, arXiv:0806.1365 [nucl-th].
[24] K. Suzuki, Prog. Theor. Phys. **68**, 246 (1982).
[25] M. Baldo and L. S. Ferreira, Nucl. Phys. A **480**, 271 (1988).
[26] Y. Tian, Z.-Y. Ma, and P. Ring, Phys. Rev. C **80**, 024313 (2009).
[27] H. Kamada *et al.*, Prog. Theor. Phys. **115**, 839 (2006).
[28] P. Bożek, D. J. Dean, and H. Müther, Phys. Rev. C **74**, 014303 (2006).
[29] J. Kuckei, F. Montani, H. Müther, and A. Sedrakian, Nucl. Phys. A **723**, 32 (2003).
[30] S. Fujii, R. Okamoto, and K. Suzuki, Phys. Rev. C **69**, 034328 (2004).
[31] F. Montani, C. May, and H. Müther, Phys. Rev. C **69**, 065801 (2004).
[32] E. N. E. van Dalen, P. Gögelein, and H. Müther, Phys. Rev. C **80**, 044312 (2009).
[33] S. K. Bogner, R. J. Furnstahl, S. Ramanan, and A. Schwenk, Nucl. Phys. A **773**, 203 (2006).
[34] J. Haidenbauer and W. Plessas, Phys. Rev. C **30**, 1822 (1984).
[35] S. K. Bogner, A. Schwenk, R. J. Furnstahl, and A. Nogga, Nucl. Phys. A **763**, 59 (2005).
[36] E. N. E. van Dalen and H. Müther, Phys. Rev. C **80**, 037303 (2009).
[37] B. A. Brown, Phys. Rev. C **58**, 220 (1998).
[38] G. Audi and A. H. Wapstra, Nucl. Phys. A **565**, 1 (1993).
[39] M. Chartier *et al.*, Phys. Rev. Lett. **77**, 2400 (1996).
[40] G. Fricke *et al.*, At. Data Nucl. Data Tables **60**, 177 (1995).
[41] G. Stoicea *et al.* (FOPI Collaboration), Phys. Rev. Lett. **92**, 072303 (2004).
[42] C. Sturm *et al.* (KaoS Collaboration), Phys. Rev. Lett. **86**, 39 (2001); C. Fuchs, A. Faessler, E. Zabrodin, and Y. M. Zheng, *ibid.* **86**, 1974 (2001); C. Fuchs, Prog. Part. Nucl. Phys. **56**, 1 (2006).
[43] S. Shlomo, V. M. Kolomietz, and G. Colò, Eur. Phys. J. A **30**, 23 (2006).
[44] T. Lesinski, T. Duguet, K. Bennaceur, and J. Meyer, Eur. Phys. J. A **40**, 121 (2009).
[45] K. Hebeler, T. Duguet, T. Lesinski, and A. Schwenk, Phys. Rev. C **80**, 044321 (2009).
[46] A. Sedrakian, T. T. S. Kuo, H. Müther, and P. Schuck, Phys. Lett. B **576**, 68 (2003).